



Collision measurements using digital image correlation techniques



Hamid Ghaednia^{a,*}, Ozdes Cermik^a, Dan B. Marghitu^a, Kamran Kardel^b

^a Department of Mechanical Engineering, Auburn University, Auburn, AL, 36849, USA

^b Department of Manufacturing Engineering, Georgia Southern University, Statesboro, GA 30460, USA

ARTICLE INFO

Keywords:

Collision
Digital image correlation
Impact duration
Velocity during the impact
Speckle pattern

ABSTRACT

In this study, the digital image correlation (DIC) techniques have been used to analyze the motion during the collisions. The spline interpolation along with two dimensional Fast Fourier Transform (FFT) cross correlation has been used in order to increase the accuracy and decrease the computation time of the method respectively. Three different examples have been analyzed: normal impact of a metal rod with a 3D printed polymer flat, oblique impact of a tennis ball with a tennis racket, and oblique impact of a lacrosse ball with a wooden flat. A speckle pattern study has been done to find the optimum pattern for the DIC technique. For the normal impact of the rod, the velocity during the impact have been measured. The normal velocity has been found by the DIC technique. For the oblique impact of the balls, the linear and angular motion have been calculated during the impact. The velocity field on the ball surface has been measured using the DIC technique. The Hough transform method has been used in combination with the measured velocity field to find the velocity of the centroid of the balls. The angular velocity during the impact has been found using the velocity field of the surface of the ball. It has been shown that the DIC technique can be used to measure the motion of colliding objects.

© 2017 Elsevier Ltd. All rights reserved.

1. Introduction

Measuring and predicting the motion of objects during the impact has been a challenge for centuries. The complexities of these measurements come from two main features of mechanical impact: short impact duration and small deformation. The impact duration is estimated to be in the order of microseconds for metals and no more than milliseconds for softer materials such as strong rubber. On the other hand, the deformation during the impact is very small for a low initial impact velocity.

There have been many efforts on measuring the motion of the objects during the impact; however, in most cases the accuracy is not high enough compared to the scale of deformation on the objects to trust the measurements. Stoianovici and Hurmuzlu [1] used a high speed camera with 1000 frames per second (fps) to track the motion of a metal rod impacting a flat. A digital camera was used to measure the velocities before and after the impact. The motion during the impact was not recorded. An electrical circuit was used to measure the contact time. The study showed that multiple impacts would occur during a single oblique impact. Minamoto and Kawamura [2] measured the impact duration and the coefficient of restitution using an electrical circuit and an image processing technique.

The image processing techniques have been used to measure the motion of the impacting objects. Although studies such as Kharaz and Gorham [3–5], Ghaednia et al. [6–10], Marghitu et al. [11], and Pfeiffer [12] measure the coefficient of restitution using image processing techniques, they are limited to the motion before and after the impact. Simple image processing methods such as tracking an object [6–8] can provide one-pixel accuracy for the position measurement. However, one-pixel accuracy is not enough when dealing with an impact problem since the displacement during the impact is smaller than the accuracy.

The motion of spheres such as different types of sport balls have been studied by many researchers. Laurent et al. [13] used a high speed camera to analyze the impact of spheres, but the measurements were limited to before and after the collisions. They used edge detection and clustering techniques in order to find the position of the spheres. They improved the accuracy with sub-pixel expansion. Goodwill et al. [14] studied the impact between a tennis ball and a racket and measured the ball rotation using an image processing technique [15]. The velocity and rotation of the ball before and after the impact were calculated automatically with a specialized software. Haake et al. [16] captured the motion of a tennis ball during the contact with a string bed at high frequency; however, no information was obtained during the impact other than the contact time. Allen et al. [17] used a high speed camera in or-

* Corresponding author.

E-mail addresses: hamid.ghaednia@auburn.edu, ghaednia.hamid@gmail.com (H. Ghaednia), ozdescermik@auburn.edu (O. Cermik), marghdb@auburn.edu (D.B. Marghitu), kkardel@georgiasouthern.edu (K. Kardel).

<http://dx.doi.org/10.1016/j.ijmecsci.2017.07.025>

Received 25 July 2016; Received in revised form 14 March 2017; Accepted 29 July 2017

Available online 10 August 2017

0020-7403/© 2017 Elsevier Ltd. All rights reserved.

der to capture the impact of a tennis ball with a racket and compared the results with finite element simulations.

Cross [18–20] studied different types of sports balls in terms of their bouncing behavior. He used a video camera at low fps rate and calculated the rotation of the ball before and after the bounce. Grip and slip phases of the bounce were visually analyzed with a high speed camera by Cross [21]. Cross [22,23] studied the oblique impact of a hollow rubber ball and measured the angular velocity of the ball during the impact. He used a manual image processing technique, which was limited to higher impact velocities. Rezaei et al. [24] studied oblique impact of a soccer ball and used a high speed camera in order to track the motion of the ball. The tracking of the ball was automatic but the accuracy was low, the error for the position of the center of the ball was 2 pixels, and no experimental result was obtained during the impact.

Numerical derivations on the position can be used to measure the velocity and acceleration (and ultimately the contact force), but numerical derivations decrease the accuracy significantly. Therefore, sub-pixel accuracy is needed for the image processing methods.

Accelerometers can be used to measure the impact characteristics. They are commonly used as an impact detection sensors for robots. These sensors can be used to measure the contact force during the impact by measuring the acceleration; however, they change the surface characteristic, which affects the contact forces especially the friction force.

The digital image correlation (DIC) methods are widely used for displacement, strain, and thermal expansion measurements [25,26]. Although DIC methods are highly accurate and need simple experimental setup, they are computationally expensive when used for several images. DIC methods have been started with the work of Peters and Ranson [27] with one-pixel accuracy and later were improved by Sutton et al. [28] for sub-pixel accuracy with a method called the coarse-fine method. Although Sutton et al. used linear interpolation between pixels, the accuracy was not enough for the strain measurements. Later, Bruck [29] introduced a revolutionary method by using the Newton–Raphson (NR) search method. Bruck [29] used bi-cubic interpolation instead of bilinear interpolation. The accuracy and the computational time of the method increased by an order of magnitude. Davis and Freeman [30], and Jin and Bao [31] developed the gradient method and the curve fitting method respectively. Both of the methods are faster than the NR search analysis; however, they are less accurate. Chen [32,33] improved the accuracy of the NR method by using spline interpolation instead of bi-cubic interpolation. Pan et al. [34–38] developed several methods to decrease the computational time of NR-DIC and provided a complete review of DIC methods in details [25].

In this paper, we focus on using the DIC method for the collision problems. Impact problems have two main complexities for image processing methods. First, there is a large number of the frames to analyze, which increases the computation time significantly. Second both large and very small displacements occur at the same time. Digital image correlation methods provide better accuracy for a video recorded with higher frequency. On the other hand, higher frequency requires longer computational time to process the videos. Spline interpolation used in [33] and Fast Fourier Transform (FFT) cross correlation methods [39–44] usually used in particle image velocimetry (PIV) are combined. The Fast Fourier Transform [44] has been employed to decrease the computation time. Spline interpolation has been used to get to sub-pixel accuracy and to capture small deformations during the impact. It was shown by Willert and Gharib [44] that the sub-pixel accuracy can be achieved in FFT correlation by implementing a Gaussian fit on the correlation peak function. We have shown later in the paper that for very small displacements direct interpolation on the interrogation windows before the FFT cross correlation is more accurate. An analysis on the speckle pattern has been also done in order to increase the accuracy of the method. To our best knowledge the DIC methods have not previously been employed to calculate the motion during the impact. Our study can be considered one of the first works to show the potential of

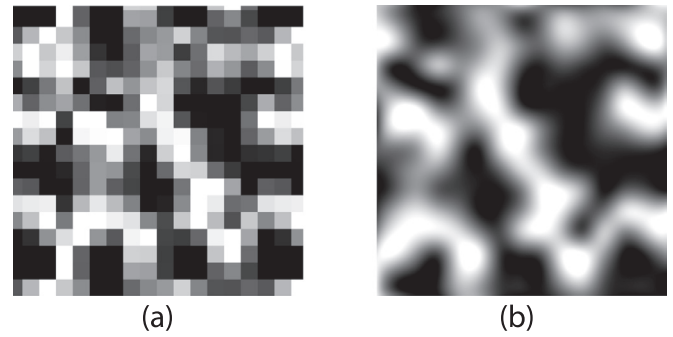


Fig. 1. Spline interpolation for a 15 × 15 pixel interrogation window (a) the original image, (b) spline interpolation with 5 extra points in between pixels.

the DIC methods to measure the linear and the angular velocities during the impact.

2. Method

The digital image correlation technique is used to calculate the displacement field on an image. The idea is to track a randomly generated pattern, called a speckle pattern. The speckle pattern is made on the objects by spraying white or black paint. Black ink has been used in this study to generate the speckle pattern on the objects. Later in this paper, a short optimization of the speckle patterns will be discussed. We use black and white images, where an 8-bit number is assigned to each pixel. The image is divided into square or circular interrogation windows depending on the type of study. The spline interpolation has been used to increase the accuracy from pixel to sub-pixel. Figure 1(a) shows an example of a spline interpolation for a 15 × 15 pixel interrogation window. A spline interpolation with 5 extra points in the middle of each two pixels has been shown in Fig. 1(b). Although increasing the number of extra points for the interpolation would improve the accuracy of the method, it would also increase the computation time drastically. For each experiment, the number of the interpolation points has been increased until the measurements converge to a constant value.

Next, FFT cross correlation [39–44] has been implemented for each of the interrogation windows to find the displacement of the center for each window during the next frames. The Fast Fourier Transform cross correlation tries to find the spacial shift between one interrogation window at one image to the counterpart interrogation window in the other image. Assuming the interrogation window in the first image to be a 2 dimensional array, $f(m, n)$ and the counterpart interrogation window in the second image to be, $g(m, n)$, one can relate these two interrogation windows via the spacial displacement function, $s(m, n)$ [44]:

$$g(m, n) = [f(m, n) * s(m, n)] + d(m, n), \tag{1}$$

where $*$ denotes the spacial convolution of the f and s , and $d(m, n)$ is the error or noise, which is the direct result of particles moving off the edges of the interrogation windows or out of plane motion of the speckle pattern. Eq. (1) can be rewritten for the discrete case as:

$$g(m, n) = \left[\sum_{k=-\infty}^{\infty} \sum_{l=-\infty}^{\infty} s(k - m, l - n) f(k, l) \right] + d(m, n). \tag{2}$$

The displacement function, $s(m, n)$ for the discrete case is the Dirac delta function $\delta(m - i, n - j)$, which is displaced from the origin by i and j . The displacement of the Dirac delta function corresponds to the average displacement of the particles in the sampled region. The statistical technique of spacial cross correlation can be used to find the displacement function for the discrete case. The correlation coefficient function can be described as:

$$\phi_{fg}(m, n) = \frac{\sum_{k=-\infty}^{\infty} \sum_{l=-\infty}^{\infty} f(k, l) g(k + m, l + n)}{\sum_{k=-\infty}^{\infty} \sum_{l=-\infty}^{\infty} f(k, l) \sum_{k=-\infty}^{\infty} \sum_{l=-\infty}^{\infty} g(k, l)}, \tag{3}$$

where higher values of ϕ show that many particles in the first image match up with the specially shifted particles in the second image. The peak position of the ϕ shows the displacement function.

Statistical Correlation method is accurate but also computationally very expensive. By neglecting the noise effect, $d(m, n)$, Eq. (1) can be rewritten with the discrete Fourier transforms of F , G , and S as:

$$g(m, n) \approx f(m, n) * s(m, n) \Leftrightarrow G(u, v) \approx F(u, v)S(u, v). \quad (4)$$

An approximation for $S(u, v)$ can be obtained using Eq. (4) if the noise can be neglected. By inversely transforming $S(u, v)$, the desired displacement function $s(m, n)$ can be obtained. Although the implementation of FFT for cross correlation is simple, the method is very sensitive to the effect of the noise, $d(m, n)$ [44]. According to Willert and Gharib [44], the displacement function needs to be measured in sub-pixel accuracy to achieve sufficient resolution in the particle displacement values. This can be done by fitting a Gaussian or other functions on the correlation peak function rather than the direct interpolation of the interrogation windows. Later in the paper, we are comparing the direct interpolation of the interrogation windows and the interpolation of the correlation peak function.

Finding the velocity field is not enough to track a certain point on an object. To study the motion of a sphere, one needs to measure the velocity of the centroid of the sphere. Therefore, the position of the centroid of the sphere is needed. A combination of position tracking method along with the DIC method is required. The Hough transform method [45,46] is one way to track the positions of the objects. In this work, the Hough transform method has been used to track the position of the centroid of the sphere, and the velocity of the center of the ball has been calculated using the measured velocity field.

3. Speckle pattern study and validation

To validate the image processing method's implementation for the linear and angular motion, a video generator has been made. A picture of the object has been used in the video generator with known angular velocity and linear motion of the centroid of the ball. Later, the generated video is analyzed using the DIC method to validate the method and its implementation. The speckle pattern on the objects is another important parameter to be analyzed. There are a few studies [47–50] for the speckle pattern for strain measurements, but to our best knowledge, there is no comprehensive study on the speckle pattern for the dynamic problems such as impact where large and small displacements and rotations can be observed together.

Figure 2 shows six different patterns that have been used for the speckle pattern study. The tennis balls Fig. 2 (a)–(d), and the lacrosse balls Fig. 2 (e) and (f) have been painted with black ink to keep the surface characteristic nearly unchanged. Patterns (a)–(d) show four different speckle sizes with three different densities from I to III. For the simplicity, we will reference balls by their indexes represented in Fig. 2. For example, Fig. 2 (a)I will be called as the ball (a)I. Balls (e) and (f) show the combination of different sizes of speckles. Balls (f) also have a few straight lines in addition to the speckles. The images have been captured with a high speed camera at 10 000 fps, which was also used for the experiments.

The speckles on the balls (a) have an average area of 4 pixels with different densities of dark pixels, with I being 9%, II being 17%, and III being 24%. For the balls (b), the average area of the speckles is 10 pixels with densities 13%, 19%, and 31% for I, II, and III, respectively. The balls (c) have average speckle areas of 20 pixels with densities 14%, 18%, and 27% for I, II, and III, respectively. The balls (d) have an average speckle areas of 250 pixels with densities 22%, 30%, 43% for I to III, respectively.

The ball (e)I has a combination of different speckle sizes from 4 to 80 pixels with a density of 54%. The combination of speckle areas is from 2 to 40 pixels for the ball (e)II. The shapes of the speckles for the balls (e) are also random, unlike the circular shapes for the other balls.

The ball (f)I has different size of speckles ranging from 4 to 20 pixels with 27% density. Speckles from 4 to 80 pixels with density of 52% are used for the ball (f)II. The balls shown in Fig. 2 have been used along with the video generator to analyze four different motions: translation in one direction, translation in two directions, pure rotation, and general motion. Six different velocities for the linear motion have been selected, $v = 0.0, 0.1, 0.5, 1.0, 1.5, 2.0$ pixel/frame. Four different angular velocities have been used for the error analysis, $\omega = 0, 1, 2, 3$ deg/frame. The error analysis has been implemented for the possible combination of these velocities for both horizontal and vertical directions and angular velocity. The digital image correlation method has been implemented with 5 points spline interpolation between pixels for all the speckle pattern types. Finally, for each speckle pattern type, 144 movies have been generated and analyzed to verify the applicability of the method for different speckle patterns.

The first case is the translation in one direction. The video is 1 fps, and the displacement rate changes from 0.1 to 2 pixel/frame. The errors for the linear motion and the rotation are shown in pixel/frame and deg/frame respectively. Figure 3 shows the mean absolute error of the displacement rate measurement for all of the balls. The ball (e)I shows the least errors with 0.02 pixel/frame in X direction, 0.03 pixel/frame in Y direction, and 0.01 deg/frame for the rotation measurement. The ball (d)III shows the largest error as expected. The balls (a)III and (b)III show around 0.03 pixel/frame error; however, the standard deviation for these two speckle types is slightly larger than ball (e)I.

The second case is the translation in two directions with 25 different velocities ranging from, $\vec{v} = 0.1\hat{i} + 0.1\hat{j}$ to $\vec{v} = 2\hat{i} + 2\hat{j}$ pixel/frame. Figure 4 shows the mean absolute error of the displacement rate for this translation case. The ball (e)II shows the least error and standard deviation with 0.02 and 0.02 pixel/frame in X and Y directions respectively and 0.005 deg/frame for the rotation. The balls (e)I, (a)III and (b)III also show acceptable errors. The balls (d)I-III show the largest error, which is similar to the first case. There is a trend in the results that the accuracy increases as the density of the dark pixels increases for the balls (a), (b), (c), (e) and (f). The method used here consists two simultaneous analyses, the Hough transform method to track the center of the ball, and the DIC to find the velocity field on the surface of the colliding objects. Both of these analysis are affected by the size and density of the speckles. As the speckle density increases the accuracy of the Hough transform method decreases, since the speckles are disrupting the edges of the objects. This decreases the accuracy of the position tracking as well as the measurement of the velocity at the center of the balls. On the other hand, Fig. 4 shows that for all three (a), (b), and (c) balls, as the density increases, the accuracy of the method increases. This comes from the fact that finding the correct peak is harder when there are less dots in each interrogation window. For the size of the speckles, however, the trend is not the same as can be seen in Fig. 4. The ball (b)3 with speckle size smaller than ball (c)3 and larger than ball (a)3 shows the most accurate results. This trend is caused by the size of the speckles increasing as the correlation peaks become more flat, therefore decreasing the accuracy of the method. Hence, there is a balance between the size and the density of the speckle patterns; density helps with the precision, while the size affects the accuracy of the method.

The third case is pure rotation of the ball with an angular velocity ranging from, $\vec{\omega} = 1\hat{k}$ to $\vec{\omega} = 3\hat{k}$ deg/frame. Figure 5 shows the mean absolute error of the rotation measurement in deg/frame. By neglecting the deformations on the ball during the impact, the ball can be assumed to be a rigid body. The relative velocity of any two interrogation windows, measured from the velocity field, can be used to calculate the angular velocity. The rotation is calculated from the velocity field by solving and averaging omega for all of the interrogation windows on the ball. Balls (e)I and (e)II show the least errors with 0.05 and 0.15 deg/frame respectively. The error in the linear velocity measurements comes from the position measurement that has been done by the Hough transform method. The balls (f)I and II, (b)III and (a)III also show acceptable errors around 0.4 deg/frame.

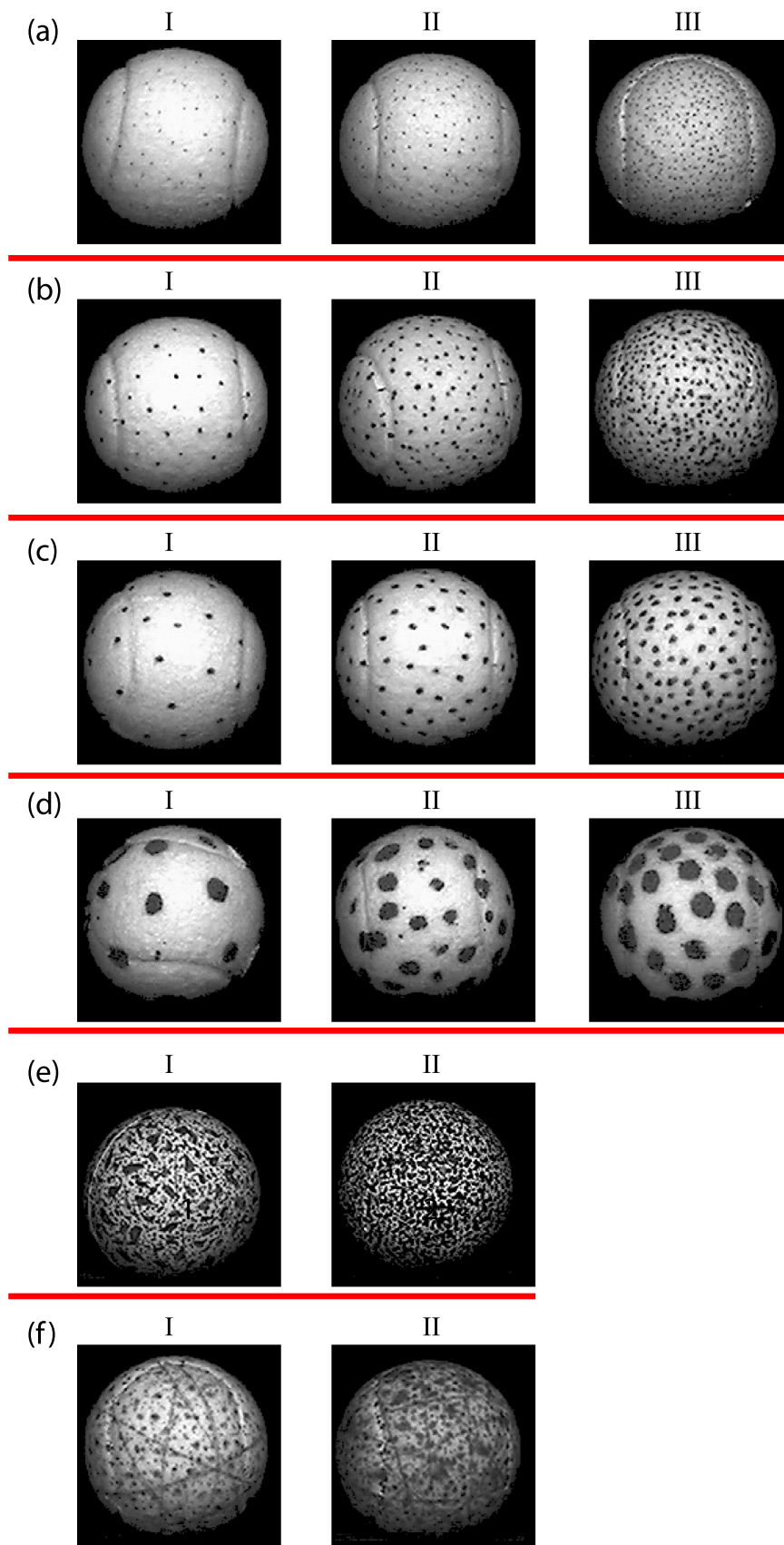


Fig. 2. Speckle patterns used in this study, (a)–(f) show different speckle patterns and indexes I to III show different densities for each speckle pattern with I and III being the least and most dense respectively.

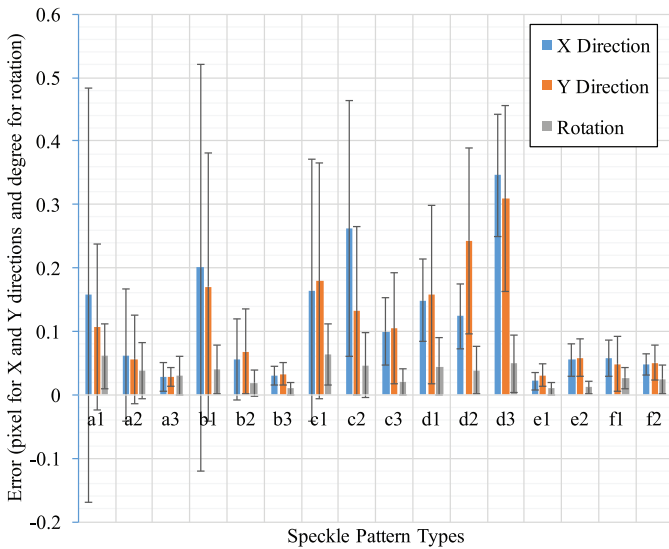


Fig. 3. Speckle pattern study for translation in one direction.

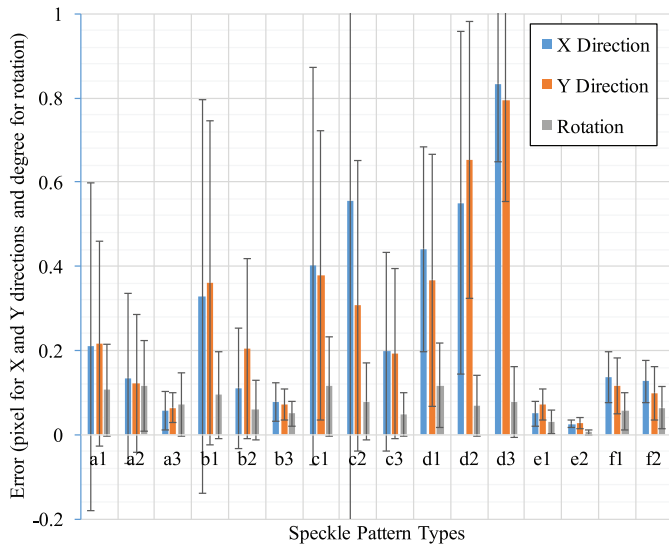


Fig. 4. Speckle pattern study for translation in two directions.

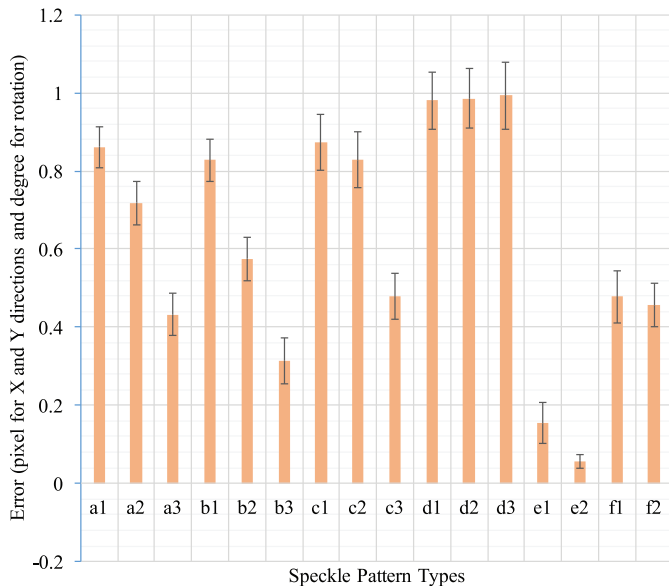


Fig. 5. Speckle pattern study for pure rotation.

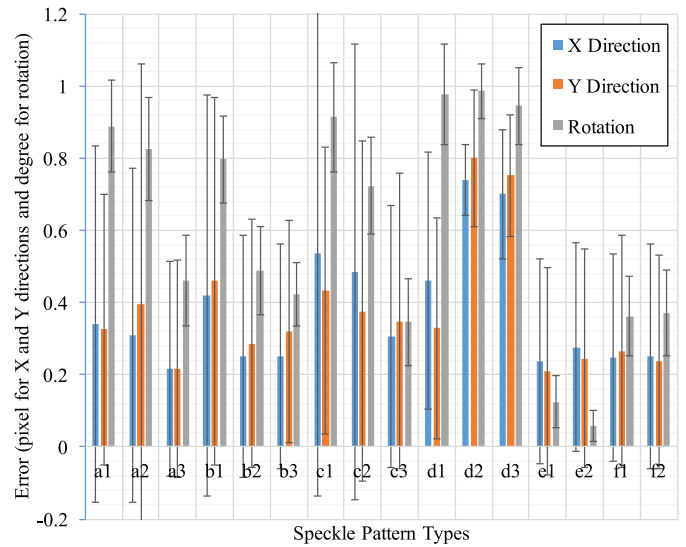


Fig. 6. Speckle pattern study for general motion.

Using circular or ring interrogation windows is another method to calculate the rotation. This method is applied for our experimental results for the impact of a tennis ball with a racket. It has been shown in this study that ring-shape interrogation windows can be a good alternative for some cases.

The final case is the general motion for 75 different velocities with the linear velocity ranging from, $\vec{v} = 0.1\hat{i} + 0.1\hat{j}$ to $\vec{v} = 2\hat{i} + 2\hat{j}$ pixel/frame, and the angular velocity ranging from, $\vec{\omega} = 1\hat{k}$ to $\vec{\omega} = 3\hat{k}$ deg/frame. Figure 6 shows the mean absolute error of the displacement rate and rotation measurement for all of the balls. It can be seen that the balls (e) and (f) perform better than the other balls for this case, especially for the rotation. The existence of linear motion and rotation causes the speckles on the balls to undergo large and small displacements. For example, if the centroid of the ball has a velocity on the positive horizontal direction, and the angular velocity is counterclockwise, top of the ball will have small displacements, while the bottom of the ball will undergo larger displacements. The bigger speckles help with peak findings during large displacements, while the smaller speckles help with the accuracy of the measurements. The ball (b)III, which contains mid-size speckles, shows acceptable results as well.

Overall, the balls (e)I and (f)II show more consistent results. These balls contain a combination of speckle sizes from 4 to 20 pixels. The balls (f) include random thin (2 pixels width) lines, which helps with the ring interrogation DIC method. The balls (f)I and (e)II have been used in our experiments.

The direct interpolation on the interrogation windows is computationally very expensive; therefore as proposed by Willert and Gharib [44], interpolation on the correlation peak function has been implemented to compare with direct interpolation of the interrogation windows. Figure 7 shows the error comparison between using the spline interpolation directly on the image or on the correlation peak.

The ball (e)2 has been used for this comparison with velocities ranging from 0.1 to 2.0 pixel/frame with intervals of 0.1 pixel/frame. The videos for this analysis have been generated numerically in order to examine the measurements. In both cases, 5 points spline interpolation has been used. For the direct interpolation on the interrogation windows, the interpolation has been made between each two pixels. On the other hand, for the correlation peak function, the interpolation has been done on ϕ_{fg} (Eq. (3)). For extremely small displacements, less than 0.5 pixel/frame, interpolation only on the correlation peak function produces significantly less accurate data. The inaccuracy comes from finding the wrong peak. Using both interpolation at a same time significantly increases the computation time.

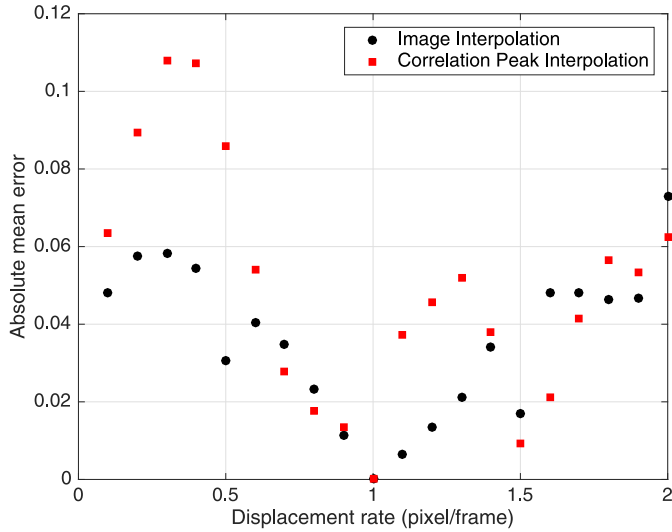


Fig. 7. Comparison between using spline interpolation directly on the image and using the interpolation on the peak correlation.

4. Experiments

The image processing methods have been employed for three different impact cases in order to verify the method’s viability for collision problems. A normal impact of a metal rod with a 3D printed industrial PLA flat, the oblique impact of a tennis ball with a tennis racket, and the oblique impact of a lacrosse ball with a rigid flat are studied. Each of these examples has their own unique challenges. The focus of this study is to find the velocity fields with high accuracy.

The impact duration is small for the normal impact of the rod with the flat, since both of the objects have relatively large stiffnesses. Therefore, the motion of the rod has been recorded with high frequency at 40,000 fps. On the other hand, for the majority of the high speed cameras the higher fps reduces the image quality.

The oblique impact of the tennis ball with the racket is the most challenging case in this study due to the deformations on both of the objects. The ball undergoes small deformations. Another challenge for this case is that a part of the tennis ball becomes invisible during the impact due to the racket frame, and that makes the image processing method much harder. The goal for this case is to measure the linear and angular velocities during the impact.

For the oblique impact of the lacrosse ball, the flat is rigid, and the ball undergoes relatively small impact deformations. Our goal is to measure the velocity field with a high accuracy. The following subsections will explain each of the experiments in detail, and compare the final results.

4.1. Test 1: normal impact of a rigid rod

Figure 8 shows the schematic of the experimental setup for the normal impact of a rigid rod with a deformable flat [51]. A round ended stainless steel rod with length, $L = 0.304$ m, diameter, $D = 0.009$ m, mass, $m = 0.255$ kg, modulus of elasticity, $E = 212$ GPa, Poisson ratio, $\nu = 0.3$, and yield strength, $S_y = 750$ MPa, has been used for the collisions. The flat is a 3D printed part made from industrial PLA with modulus of elasticity, $E = 3.2$ GPa, Poisson ratio, $\nu = 0.36$, and yield strength, $S_y = 37$ MPa. The flat is screwed to a massive metal flat, which itself has been fixed to a massive surface. Two electromagnet solenoids have been used to hold and release the rod from a certain height. A high speed digital camera with 40,000 fps has been used to record the collision.

For this test, we tracked the position of the rod with a regular image processing tracking method and found the velocity field on part of the rod during the impact as shown in Fig. 9. The rod has been painted in

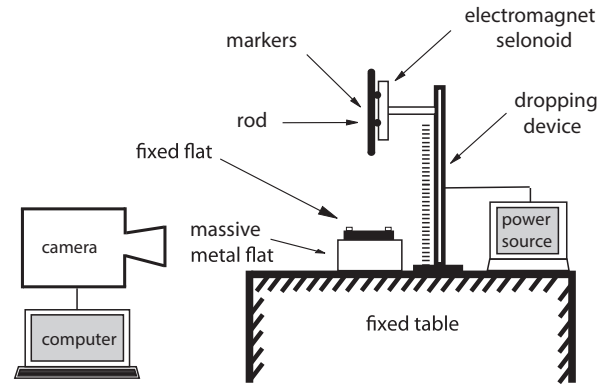


Fig. 8. Experimental setup for the normal impact of a rigid rod and deformable flat.

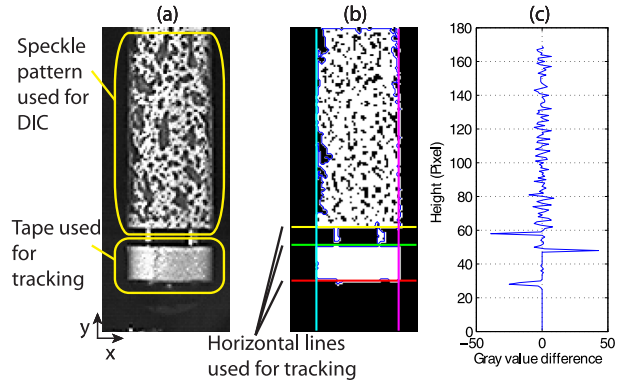


Fig. 9. (a) Original image of the rod, (b) modified version of the rod with pure black and white and horizontal lines, (c) gray value difference.

black and two silver coated adhesive tapes have been attached to the rod (see Fig. 9(a)). The bottom tape remained clean to be used for the position tracking, and the top tape has been painted randomly to create a speckle pattern to be used for the DIC method. The position of three horizontal lines, shown in Fig. 9(b), including the bottom edge of the bottom tape, the top edge of the bottom tape, and the bottom edge of the top tape, have been measured in order to track the position of the rod. The image has been changed to pure black and pure white in order to find these lines as seen in Fig. 9(b). Let each frame to be a 2D array, $m \times n$, with 8-bit gray values for each pixel, $g(x, y)$ where x and y are the horizontal and vertical coordinates respectively. Next, the first derivations of the gray value in horizontal and vertical directions have been found and summed up for each column and row, respectively:

$$\chi_h(y) = \sum_{x=1}^n \frac{\partial g(x, y)}{\partial y}, \quad \chi_v(x) = \sum_{y=1}^m \frac{\partial g(x, y)}{\partial x}, \quad (5)$$

where χ is a coefficient we defined, and its magnitude increases at the edges, and indexes h and v refer to the horizontal and vertical directions respectively. Figure 9(c) shows χ_h for Fig. 9(b). Three local maximums from height 20 to 60 pixels show the edges that we were looking for. The vertical lines as seen in Fig. 9(b) show the boundary of the rod.

Figure 10 shows the position vs. time for a collision of the same rod recorded at 40,000 fps, with an initial velocity, $v_i = -1.05$ m/s, and a final velocity, $v_f = 0.71$ m/s. The accuracy of the regular image processing methods is one pixel, and this is the main problem for a phenomenon like collision because the impact duration and displacements are small. Since high frequency is used for these experiments, several frames show the same position at this accuracy. This makes the calculation of the velocity from the position of the rod by numerical derivation harder. Therefore, the DIC method is needed to find the velocity.

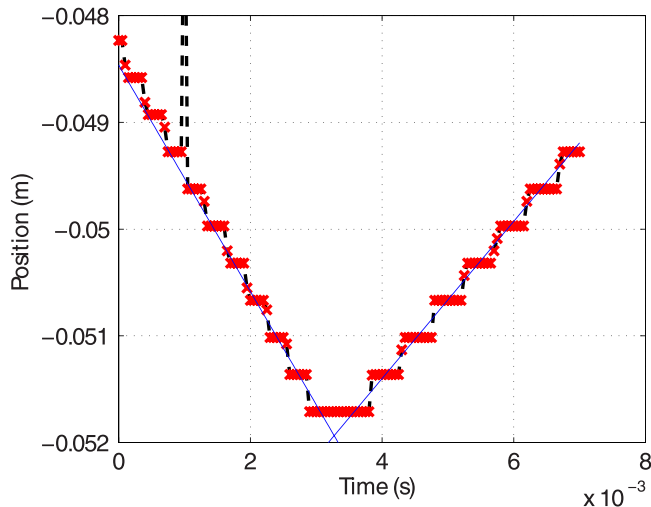


Fig. 10. Position of the rod analyzed with regular image processing method.

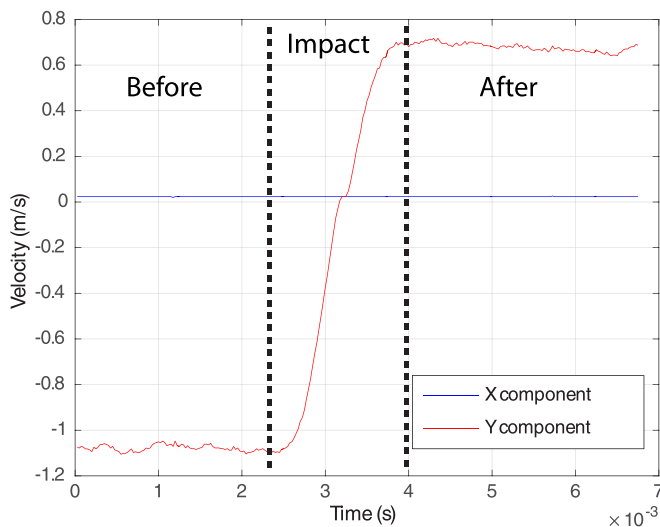


Fig. 11. Velocity of the rod measured by the DIC method.

Figure 11 shows the velocity measurements using the DIC method for the same experiment shown in Fig. 10. It can be seen that the velocity has been measured with a good accuracy. The change in velocity during the impact can be seen as well. The impact starts at $t = 2.475$ ms with initial velocity, $v_i = -1.084$ m/s, and continues to $t = 3.875$ ms with final velocity, $v_f = 0.6873$ m/s. An interesting phenomenon happens when the velocity reaches zero. The velocity stays at zero for a fraction of a millisecond and starts increasing again. The reason for this phenomenon may be the error in the measurements. We are not able to capture very small displacements less than 0.1 pixel due to the quality of our camera. It should be noted that we increased the number of interpolation points from 5 to 10, and the measurements still showed the same results. We also increased the time intervals in the image processing by comparing each frame from 5th to next 15th frame, and it still gave us exactly the same results.

4.2. Test 2: oblique impact of a tennis ball with a racket

In this case, the low velocity oblique impact of a tennis ball with a tennis racket has been studied. Figure 12 shows the schematic of the setup. Tennis balls with the diameter of 0.067 m and the mass of 0.0567 kg have been used for the experiments. The tennis ball is held and released by a robotic arm for consistent drops. The ball has been released from a certain height without an initial angular velocity. The

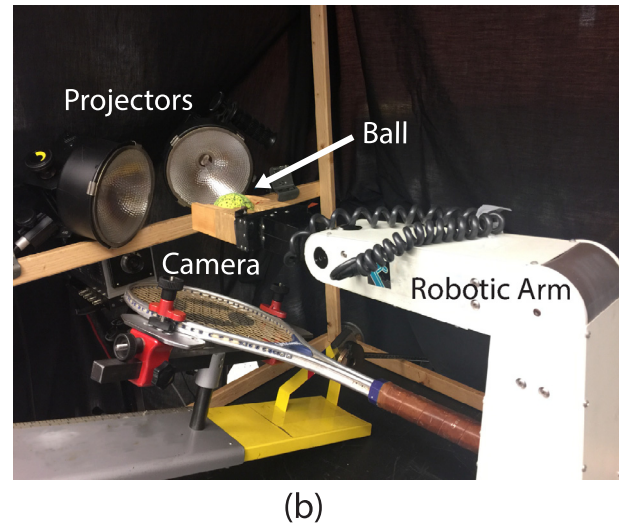
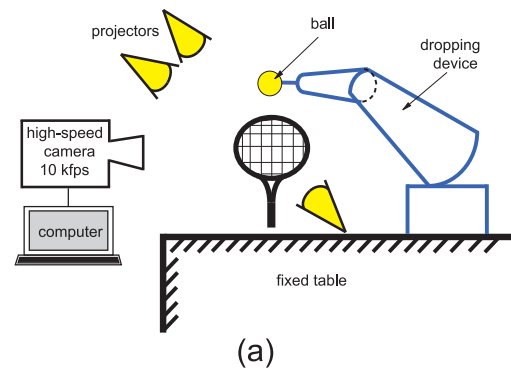


Fig. 12. Experimental setup for the impact of a tennis ball with a racket, (a) schematic view, (b) real view.

collision has been recorded with a high speed camera at 10 000 fps. The camera is placed horizontally 0.8 m from the collision plane. Three projectors have been used to provide the required light for the setup. The impact angle, β , is the angle of the tennis racket with the horizontal axis. The racket has been clamped to a massive supporting device, and a tripod is used to set the angle of the device accurately. The end of the supporting device has been also clamped to the table to reduce the vibrations of the racket. The ball with speckle pattern shown in Fig. 2(f) has been used for the experiments.

The resolution of the high speed camera is 512×512 pixels when recording with 10 000 fps, in which the tennis ball has a diameter of, $D = 114$ pixels. For this study a lens with, focusing range: $1 - \infty$ m, focal length: 12.5 – 75 mm, aperture ring: 1.2 – 16, maximum aperture: 1:1.2, and filter size: 54 mm has been used. The Hough transform method has been used to track the centroid of the ball. One of the challenges for the image processing of this case is that during the impact a part of the ball is covered behind the racket as seen in Fig 13. Although the Hough transform method is capable of measuring the position of the centroid of the ball even when part of the ball is hidden, the accuracy of the DIC method, especially for rotation measurements decreases.

Figure 13 shows the image processing procedure for tracking the centroid of the ball, measuring the velocity field and rotation. Figure 13(a) shows the ball at the beginning of the impact, the left picture shows the original frame, and the right picture shows the measured velocity field using the DIC method. The Hough transform is used to find the boundary and centroid of the ball as shown on the left picture in Fig. 13(a). It can be seen that Hough transform method can find the boundary and the centroid of the ball even when part of the ball is hidden behind the tennis racket.

The picture on the right side of Fig. 13(a) shows the velocity field measured by the DIC method at the beginning of the impact. It should

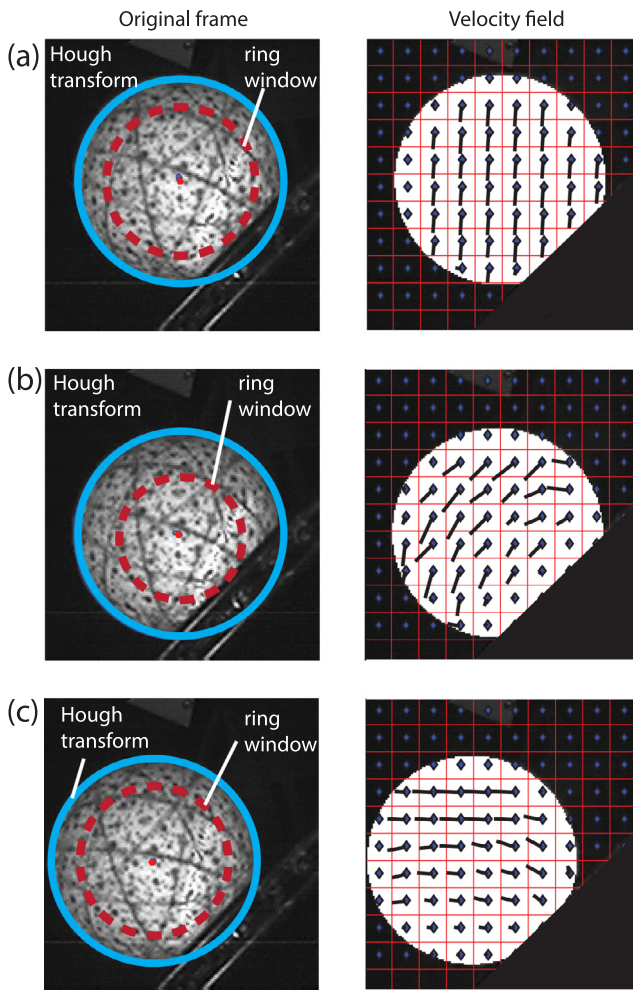


Fig. 13. Original frames and the velocity field of the impact of a tennis ball with a racket, calculated by DIC, (a) the beginning of the impact, (b) during the impact, (c) the end of the impact.

be noted that the surface of the ball has been changed to pure white just for clarification purposes. The velocity at the center of each of the interrogation windows has been calculated and represented with a line in the picture (the length of each line is the scaled displacement of the center of each interrogation window). The center of each interrogation window is represented with a diamond shape marker. Each line starts from the center of the interrogation windows and shows the displacement of that window during the next time interval. The velocity field shows constant downward velocity for all of the windows, which is as expected.

For the rotation measurement of the ball a circular ring interrogation window centered at the centroid of the ball is used, as shown in the left picture of Fig. 13. The radius of this ring interrogation window is the distance from the centroid of the ball to the edge of the racket. It has to be noted that the radius of the window shrinks during the impact as larger part of the ball hides behind the racket, see Fig. 13(b).

For this case, it was observed that the circular interrogation window DIC is working better than averaging the angular velocity for the square interrogation windows. This may be due to the fact that during the impact a part of the ball is hidden behind the racket. A circular interrogation window with a radius equal to the distance of the centroid of the ball from the edge of the racket has been used to measure the rotation, as seen in Fig. 13. Two-point spline interpolation has been used to increase the accuracy. It was observed that adding lines to the speckle pattern increases the accuracy of the circular interrogation window DIC.

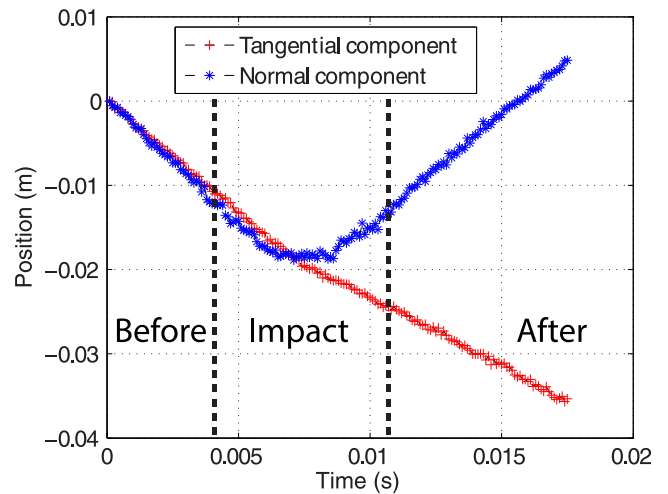


Fig. 14. Position of the centroid of the ball measured by the Hough transform method.

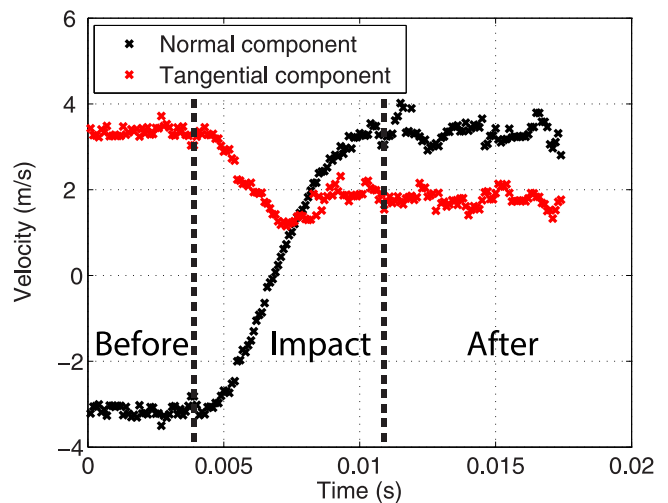


Fig. 15. Velocity of the centroid of the ball measured with DIC method.

Figure 13(b) shows the tennis ball during the impact. Same as Fig. 13(a) the Hough transform is used to find the boundary, and centroid of the ball and the circular interrogation window is used for the rotation measurement. The right picture in Fig. 13(b) shows the velocity field during the impact. The velocity field shows smaller values for the points close to the contact point and larger as it gets further from the contact point, which shows the rotation of the ball during the impact. Figure 13(c) shows the velocity field at the end of the impact. The velocity field clearly shows the bounce and the counter clockwise rotation.

Figure 14 shows the position of the centroid of the ball for the oblique impact of a tennis ball with an impact angle, $\beta = 45^\circ$, normal and tangential initial velocity, $v_n = v_t = 3.2$ m/s respectively. The measurements have been done by using the Hough transform method to track the centroid for a collision recorded at 10,000 fps. The time when the rebound starts can be measured from the normal component of the position in Fig. 14. Even though, the measurements show good results, the precise initiation of collision cannot be detected easily. The tangential component shows a decrease in the velocity after the impact as expected.

Although, the position measured by the Hough transform shows acceptable results, the first derivation of the position in order to calculate the velocity is very noisy. Therefore, the velocity of the center has to be calculated with the DIC method. Figure 15 shows the measured velocity of the centroid of the ball for the same collision as Fig. 14, with the impact angle, $\beta = 45^\circ$, and normal and tangential initial velocity,

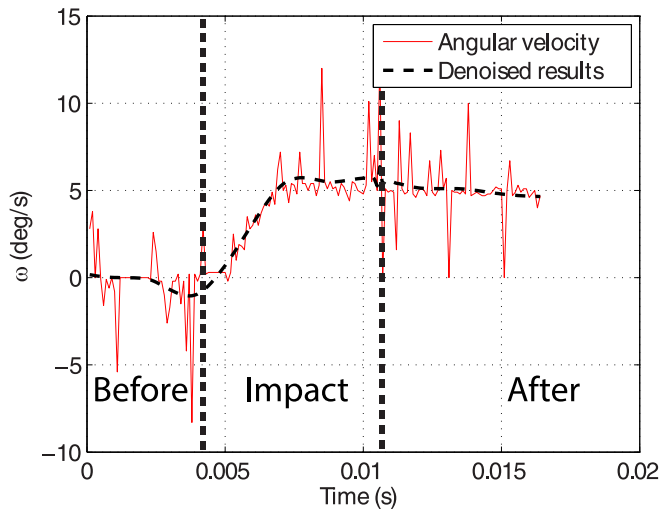


Fig. 16. Angular velocity of the tennis ball calculated by DIC method.

$v_n = v_t = 3.2$ m/s. From the normal velocity it can be seen that the impact starts at $t = 4$ ms. The restitution starts at $t = 7$ ms, and ends at $t = 11$ ms. The normal component of the velocity of the centroid of the ball shows a smooth trend during the impact. The tangential component of the velocity is considered to be positive in x-direction. The tangential component shows an interesting phenomena. When the impact starts, $t = 4$ ms, the tangential component starts decreasing to a certain point, $t = 7.2$ ms and stays constant until $t = 8$ ms. After this point, the tangential velocity starts increasing until $t = 9$ ms. Although this result is interesting for understanding the nature of contact force during the impact, one should consider that Fig. 15 shows the velocity of the centroid of the ball, therefore the angular velocity is needed as well to be able to discuss the contact forces during the impact.

Figure 16 shows the angular velocity of the ball during the same impact as seen in Figs. 14 and 15. Although, there is some noise in the measurements due to the low resolution of the high speed camera, the results are acceptable to use for understanding the nature of the friction forces. It can be seen that the impact starts at $t = 4$ ms, the angular velocity starts from zero and increases during the impact until $t = 7.2$ ms, and stays constant around $\omega = 5$ rad/s.

Figures 15 and 16 show that the collision can be divided into three phases in terms of the tangential motion. The first phase starts at $t = 4$ ms. The tangential velocity of the centroid of the ball decreases and the angular velocity increases. This phase continuous until $t = 7.2$ ms. During the second phase, from $t = 7.2$ ms to $t = 8$ ms, both the tangential, and the angular velocity of the ball stay constant which means there is no tangential impulse acting on the ball. For the third phase, from $t = 8$ ms to $t = 10$ ms, the angular velocity stays constant, which means there cannot be any torque acting on the ball. At the same time, the tangential velocity of the centroid of the ball increases. This can be only explained by the effect of deformations on the strings, which can change the nature of the friction force from sliding to rolling friction. Modeling and predicting the motion of objects during the collision needs more detailed studies on the deformations of the objects during the impact.

4.3. Test 3: oblique impact of a lacrosse ball with a rigid flat

The last case is the low velocity oblique collision of a lacrosse ball with a rigid flat. Figure 17 shows the schematic of the experimental setup. A wooden flat has been clamped to a massive metal flat, which is attached to a tripod that controls the angle of the impact. The metal flat is clamped to the massive table, and the tripod has been fixed to reduce the vibrations during the impact. The impact angle is measured from

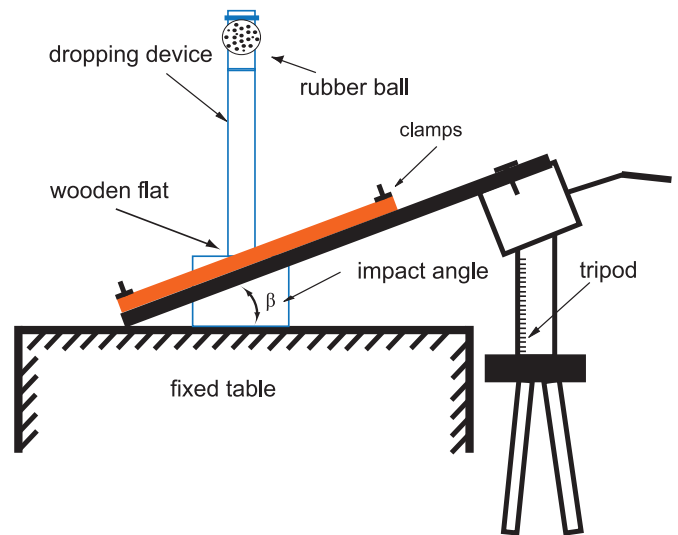


Fig. 17. Schematic of the experimental setup for the impact of a lacrosse ball with a rigid flat.

the horizontal axis. The lacrosse ball has a diameter of, $D = 63.25$ mm with mass, $m = 145.66$ gr.

To perform consistent drops with the desired initial height, a solenoid has been used to hold and release the ball. A small piece of metal has been glued to the top of the ball to be attached to the dropping device (the mass of the metal piece is very small compared to the ball). The collision is captured by the high speed camera at 10,000 fps. The camera is placed 0.4 m from the collision plane. Projectors with 1000 W have been used to provide the necessary light for the camera. The ball with speckle pattern shown in Fig. 2(e)II is used for the experiments. The resolution of the high speed camera is 512×512 pixels when recording with 10,000 fps, in which the lacrosse ball has a diameter of, $D = 123$ pixels. For this study a lens with, focusing range: $0.25 - \infty$ m, focal length: 25 mm, maximum aperture: 1: 1.6, and filter size: $\phi 25.5$ mm, has been used.

Figure 18 shows the lacrosse ball during the collision for the impact angle, $\beta = 19^\circ$, and initial velocity, $v_i = 1.80$ m/s. The ball starts with a positive initial tangential velocity (positive tangential axis is toward the right). The camera has been tilted such that the flat lays on the horizontal axis in this experiment. The Hough transform has been used to track the centroid of the ball during the collision, Fig. 18(a)–(c). The lacrosse ball undergoes small elastic deformations during the impact, which affect the accuracy of the Hough transform method. Digital image correlation method described in the last section is used with 5 points spline interpolation in order to find the velocity field on the surface of the ball, with the assumption of no out of plane motion. The velocity field shows clockwise rotation, as expected.

The position of the centroid of the ball has been measured using the Hough transform method. To improve the accuracy of the Hough transform, the boundary of the ball has been found, changed to a different color, and a filter has been applied to the ball. Because of the sharp difference between the boundary and the ball, the Hough transform method is able to measure the radius of the ball easier. Figure 18(a) shows the image from Hough transform for the centroid and the boundary of the ball at the beginning of the impact. Figure 18(b) shows the velocity distribution on the surface of the ball during the impact calculated by the DIC method with 5-point spline interpolation. The camera is tilted 19° to match the local coordinates. This change provides a higher number of pixels in the vertical direction. The results show a larger velocity field on the top left of the ball and smaller on the right, which shows a clockwise rotation as expected. Figure 19 shows the position of the centroid of the ball during the collision calculated by Hough transform.

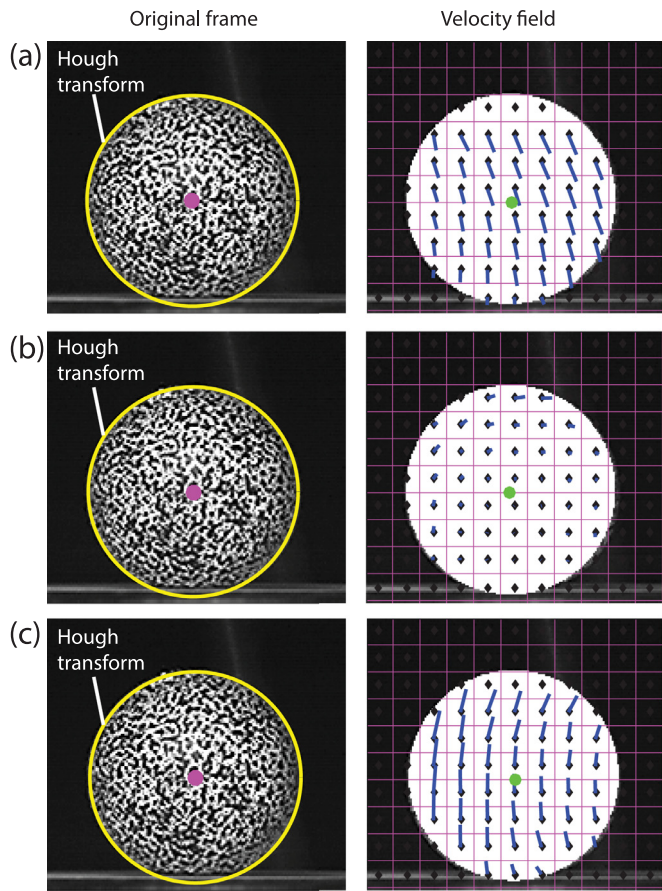


Fig. 18. Original frames and the velocity field of the impact of a lacrosse ball with a flat, calculated by DIC, (a) beginning of the impact, (b) during the impact, (c) end of the impact.

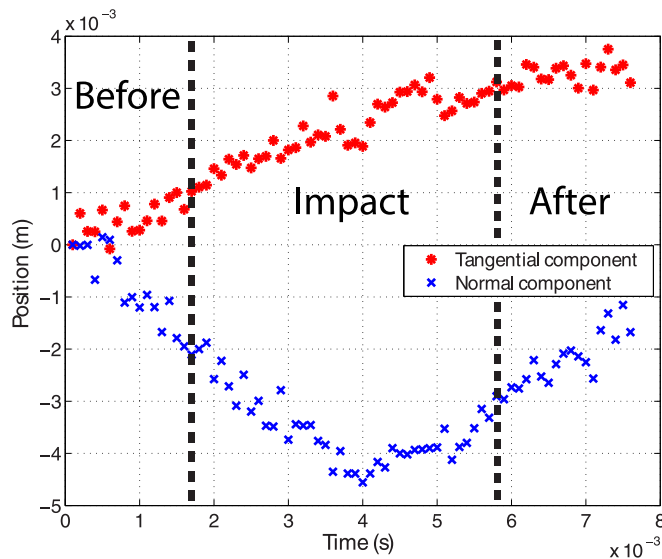


Fig. 19. Position of the centroid of the ball measured by the Hough transform.

The tangential component of the position of the ball increases during the impact where the increase rate before the impact is larger than after the impact, as expected. The normal component of the position of the ball decreases until the maximum compression and increases for the rest of the collision. Although the accuracy of the method is acceptable for the position analysis, the first derivation will result in significant noise. One

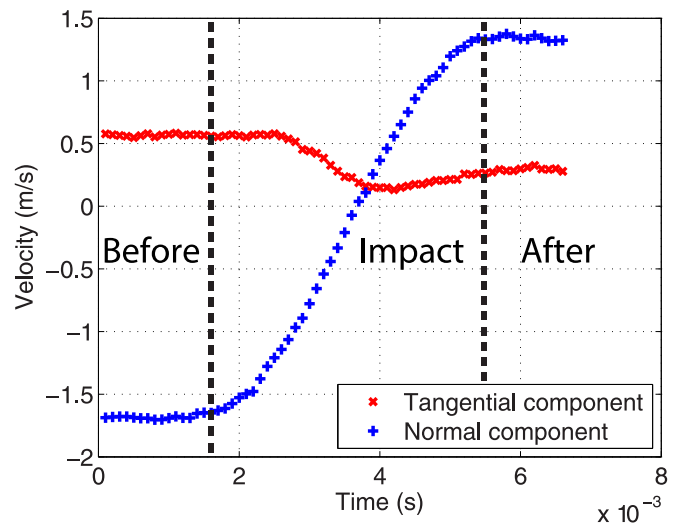


Fig. 20. Normal and tangential velocities of the centroid of the ball found by DIC method.

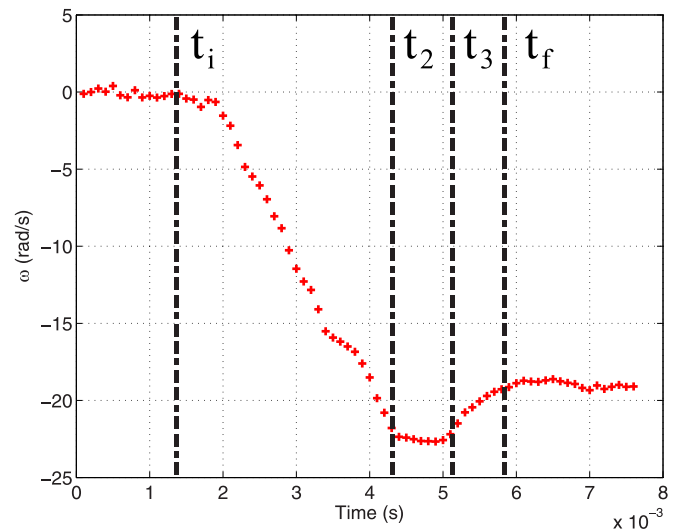


Fig. 21. The angular velocity of the ball calculated from analysis of the velocity field on the surface of the ball.

should consider that the total displacement shown in the plot is small, about 4 mm, for the normal and tangential components.

Figure 20 shows the velocity of the centroid of the ball. The velocity has been found by interpolation of the velocity field calculated by the DIC method at the position of the centroid measured by the Hough transform. The initial normal velocity is $v_n = -1.69$ m/s and the collision starts at $t_i = 1.4$ ms. At this instant the normal velocity starts increasing until $t_f = 5.8$ ms, with normal velocity after the impact $v_n = 1.35$ m/s. The maximum compression occurs at $t = 3.7$ ms, which matches the results from the position analysis shown in Fig. 19.

An interesting phenomenon is observed for the tangential velocity of the centroid of the ball. The tangential velocity starts with $v_t = 0.57$ m/s and decreases when the collision starts; however, the decrease in the velocity stops at $t_2 = 4.3$ ms. At this instant, the velocity of the contact is zero, therefore, there is no friction force affecting the centroid. This also matches with the previous speculations in the studies of rigid body collision. After this point, from $t_2 = 4.3$ ms to $t_3 = 5.8$ ms, the tangential velocity increases at a very slow but steady rate, which indicates a small net tangential force on the center of the ball.

Figure 21 shows the angular velocity of the ball during the impact. One can observe an interesting phenomenon happening at the second phase of the collision. The impact starts approximately at $t_i = 1.4$ ms,

and the magnitude of the angular velocity increases until $t_2 = 4.3$ ms. From $t_2 = 4.3$ ms to $t_3 = 5.1$ ms, the angular velocity stays constant, and after this point it decreases until the end of the impact at $t_f = 5.8$ ms. One can conclude from both linear and angular velocity that the friction force during impact is not fully sliding, fully sticking or even sliding and then sticking. Our results can be used to study the friction force during the impact, which has been the concern of many researchers for many years.

5. Conclusion

In this study a new implementation of the DIC method for the collision problems has been presented. The spline interpolation along with FFT 2D cross correlation has been used for the displacement measurements. A brief study has been done on the effect of the speckle pattern on the accuracy of the DIC method for the impact problems. Generated videos with known velocities have been used to verify the implementation of the method. The method aims to measure linear and angular motion of the objects. Three experiments have been designed and studied: normal impact of a rigid rod with a deformable surface, oblique impact of a tennis ball with a tennis racket, and oblique impact of a lacrosse ball with a rigid flat.

For the normal impact of the rigid rod, the method has been shown to be able to measure the velocity during the impact. In the second experiment, the oblique impact of the tennis ball with a tennis racket has been studied. The position of the centroid of the ball has been measured using the Hough transform method. The linear and angular velocities of the ball have been measured using the DIC method. For the angular velocity, circular interrogation windows have been used instead of square windows. The image processing method shows acceptable accuracy for both the linear and angular velocity measurements. For the third experiment, the impact of a deformable lacrosse ball with a rigid body is analyzed. The position of the centroid of the ball is measured using the Hough transform method, and the linear and angular velocities have been calculated by using the square interrogation windows in the DIC methods.

It has been shown in this study that DIC methods are able to capture the characteristics of collisions. The results from the measurements show interesting facts about the motion of the objects during the collision. These results can later be studied to understand the nature of the normal and tangential forces during the collisions. The accuracy of the studied method can be improved by either a high speed camera with a better resolution, higher frequency, or using more advanced DIC methods.

References

- [1] Stoianovici D, Hurmuzlu Y. A critical study of the applicability of rigid-body collision theory. *J Appl Mech* 1996;63(2):307–16.
- [2] Minamoto H, Kawamura S. Effects of material strain rate sensitivity in low speed impact between two identical spheres. *Int J Impact Eng* 2009;36(5):680–6.
- [3] Kharaz A, Gorham D, Salman A. Accurate measurement of particle impact parameters. *Measur Sci Technol* 1999;10(1):31.
- [4] Gorham D, Kharaz A. The measurement of particle rebound characteristics. *Powder Technol* 2000;112(3):193–202.
- [5] Kharaz A, Gorham D, Salman A. An experimental study of the elastic rebound of spheres. *Powder Technol* 2001;120(3):281–91.
- [6] Ghaednia H, Marghitu DB, Jackson RL. Predicting the permanent deformation after the impact of a rod with a flat surface. *J Tribol* 2015;137(1):011403.
- [7] Ghaednia H, Cermik O, Marghitu DB. Experimental and theoretical study of the oblique impact of a tennis ball with a racket. *Proc Inst Mech Eng Part P: J Sports Eng Technol* 2015. 1754337114567490.
- [8] Ghaednia H, Cermik O, Marghitu DB. Experimental and theoretical analysis of the elasto-plastic oblique impact of a rod with a flat. *Int J Impact Eng* 2015;86:307–17.
- [9] Ghaednia H, Pope SA, Jackson RL, Marghitu DB. A comprehensive study of the elasto-plastic contact of a sphere and a flat. *Tribol Int* 2016;93:78–90.
- [10] Ghaednia H, Marghitu DB. Permanent deformation during the oblique impact with friction. *Arch Appl Mech* 2016;86(1-2):121–34.
- [11] Marghitu DB, Cojocar D, Jackson RL. Elasto-plastic impact of a rotating link with a massive surface. *Int J Mech Sci* 2011;53(4):309–15.
- [12] Pfeiffer F. Impacts with friction: structures, energy, measurements. *Arch Appl Mech* 2016:1–21.
- [13] Labous I, Rosato AD, Dave RN. Measurements of collisional properties of spheres using high-speed video analysis. *Phys Rev E* 1997;56(5):5717.
- [14] Goodwill S, Haake S. Spring damper model of an impact between a tennis ball and racket. *Proc Inst Mech Eng Part C: J Mech Eng Sci* 2001;215(11):1331–41.
- [15] Goodwill S, Douglas J, Miller S, Haake S. Measuring ball spin off a tennis racket. In: *The engineering of sport 6*. Springer; 2006. p. 379–84.
- [16] Haake S, Carre M, Goodwill S. The dynamic impact characteristics of tennis balls with tennis rackets. *J Sports Sci* 2003;21(10):839–50.
- [17] Allen T, Haake S, Goodwill S. Comparison of a finite element model of a tennis racket to experimental data. *Sports Eng* 2009;12(2):87–98.
- [18] Cross R. Enhancing the bounce of a ball. *Phys Teacher* 2010;48(7):450–2.
- [19] Cross R. Measurements of the horizontal coefficient of restitution for a superball and a tennis ball. *Am J Phys* 2002;70(5):482–9.
- [20] Cross R. Grip-slip behavior of a bouncing ball. *Am J Phys* 2002;70(11):1093–102.
- [21] Cross R. Impact behavior of a superball. *Am J Phys* 2015;83(3):238–48.
- [22] Cross R. Oblique bounce of a rubber ball. *Exper Mech* 2014;54(9):1523–36.
- [23] Cross R. Behaviour of a bouncing ball. *Phys Educ* 2015;50(3):335.
- [24] Rezaei A, Verhelst R, Van Paepegem W, Degrieck J. Finite element modelling and experimental study of oblique soccer ball bounce. *J Sports Sci* 2011;29(11):1201–13.
- [25] Pan B, Qian K, Xie H, Asundi A. Two-dimensional digital image correlation for in-plane displacement and strain measurement: a review. *Measur Sci Technol* 2009;20(6):062001.
- [26] Sun Y, Pang JH, Shi X, Tew JR. Thermal deformation measurement by digital image correlation method. In: *Proceedings of the tenth intersociety conference on thermal and thermomechanical phenomena in electronics systems*, 2006. IEEE; 2006. p. 921–7.
- [27] Peters W, Ranson W. Digital imaging techniques in experimental stress analysis. *Opt Eng* 1982;21(3):213427.
- [28] Sutton M, Wolters W, Peters W, Ranson W, McNeill S. Determination of displacements using an improved digital correlation method. *Image Vis Comput* 1983;1(3):133–9.
- [29] Bruck H, McNeill S, Sutton MA, Peters W. Digital image correlation using Newton-Raphson method of partial differential correction. *Exper Mech* 1989;29(3):261–7.
- [30] Davis CQ, Freeman DM. Statistics of subpixel registration algorithms based on spatiotemporal gradients or block matching. *Opt Eng* 1998;37(4):1290–8.
- [31] Jin G, Yao X, Bao N. Applications of speckle metrology to vibration and deformation measurements of electronic devices. In: *Proceedings of the seventh intersociety conference on thermal and thermomechanical phenomena in electronic systems*, 2. IEEE; 2000. p. 253–5.
- [32] Chen J, Zhang X, Zhan N, Hu X. Deformation measurement across crack using two-step extended digital image correlation method. *Opt Lasers Eng* 2010;48(11):1126–31.
- [33] Chen J, Xia G, Zhou K, Xia G, Qin Y. Two-step digital image correlation for micro-region measurement. *Opt Lasers Eng* 2005;43(8):836–46.
- [34] Pan B, Asundi A, Xie H, Gao J. Digital image correlation using iterative least squares and pointwise least squares for displacement field and strain field measurements. *Opt Lasers Eng* 2009;47(7):865–74.
- [35] Pan B. Reliability-guided digital image correlation for image deformation measurement. *Appl Opt* 2009;48(8):1535–42.
- [36] Pan B, Li K. A fast digital image correlation method for deformation measurement. *Opt Lasers Eng* 2011;49(7):841–7.
- [37] Pan B, Dafang W, Yong X. Incremental calculation for large deformation measurement using reliability-guided digital image correlation. *Opt Lasers Eng* 2012;50(4):586–92.
- [38] Pan B, Li K, Tong W. Fast, robust and accurate digital image correlation calculation without redundant computations. *Exper Mech* 2013;53(7):1277–89.
- [39] Duda RO, Hart PE. *Pattern classification and scene analysis*, 3. Wiley New York; 1973.
- [40] Richards JA, Richards J. *Remote sensing digital image analysis*, 3. Springer; 1999.
- [41] Westerweel J, Dabiri D, Gharib M. The effect of a discrete window offset on the accuracy of cross-correlation analysis of digital piv recordings. *Exper Fluids* 1997;23(1):20–8.
- [42] Westerweel J. Fundamentals of digital particle image velocimetry. *Measur Sci Technol* 1997;8(12):1379.
- [43] Westerweel J. Theoretical analysis of the measurement precision in particle image velocimetry. *Exper Fluids* 2000;29:S003–12.
- [44] Willert CE, Gharib M. Digital particle image velocimetry. *Exper Fluids* 1991;10(4):181–93.
- [45] Hough PV. *Method and means for recognizing complex patterns*. Technical Report; 1962.
- [46] Ballard DH. Generalizing the hough transform to detect arbitrary shapes. *Pattern Recog* 1981;13(2):111–22.
- [47] Bossuyt S. Optimized patterns for digital image correlation. In: *Imaging methods for novel materials and challenging applications*, 3. Springer; 2013. p. 239–48.
- [48] Pan B, Qian K, Xie H, Asundi A. On errors of digital image correlation due to speckle patterns. In: *Proceedings of the international conference on experimental mechanics 2008 and seventh asian conference on experimental mechanics*. International Society for Optics and Photonics; 2008. p. 73754Z.
- [49] Collette S, Sutton M, Miney P, Reynolds A, Li X, Colavita P, et al. Development of patterns for nanoscale strain measurements: I. fabrication of imprinted au webs for polymeric materials. *Nanotechnology* 2004;15(12):1812.
- [50] Lecomte D, Smits A, Bossuyt S, Sol H, Vantomme J, Van Hemelrijck D, et al. Quality assessment of speckle patterns for digital image correlation. *Opt Lasers Eng* 2006;44(11):1132–45.
- [51] Kardel K, Ghaednia H, Carrano AL, Marghitu DB. Experimental and theoretical modeling of behavior of 3d-printed polymers under collision with a rigid rod. *Additive Manuf* 2017;14:87–94.